ACS Catalysis

Research Article

pubs.acs.org/acscatalysis

Ensemble Site Requirements for Oxidative Adsorption of Methanol and Ethanol on Pt Membrane Electrode Assemblies

Sara E. Evarts,[†] Ian Kendrick,[†] Britta L. Wallstrom,[‡] Thomas Mion,[§] Mehdi Abedi,[∥] Nicholas Dimakis,[§] and Eugene S. Smotkin*,[†]

[†]Department of Chemistry and Chemical Biology, [‡]Department of Chemical Engineering, and [∥]Department of Mechanical and Industrial Engineering, Northeastern University, 360 Huntington Avenue, Boston, Massachusetts 02115, United States

[§]Department of Physics and Geology, University of Texas-Pan American, 1201 W. University Drive, Edinburg, Texas 78539, United States

Supporting Information

ABSTRACT: The ensemble site requirements for the oxidative adsorption of methanol and ethanol on platinum based membrane electrode assemblies in operating liquid feed fuel cells were measured by CO stripping voltammetry. At 30 °C and 0.2 V vs reference hydrogen electrode (RHE), the CO_{ads} coverage from directly dosed CO (CO_{CO}), methanol (CO_{MeOH}), and ethanol (CO_{EtOH}) are 94%, 49%, and 39%, respectively. At 50 °C the CO_{MeOH} and CO_{EtOH} approach equality. The ratio of CO_{EtOH}/CO_{MeOH} was simulated with assumed ensemble site requirements of 3 and 2 for ethanol and methanol respectively. Experimental and simulated ratios of 0.79 and 0.78 suggest that high surface area fuel cell Pt catalysts at 30 °C have adsorption properties similar to that of a Pt (100) surface. Potential dependent infrared spectroscopy of CO_{MeOH} and CO_{EtOH} from flash evaporated aqueous alcohols delivered to a 50 °C fuel cell show lower CO_{EtOH} relative to CO_{MeOH} with Stark tuning rates below 10 cm^{-1}/V.

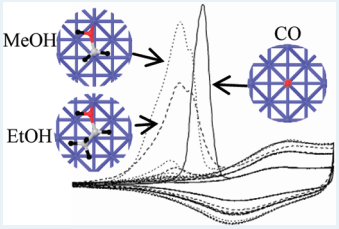

KEYWORDS: *platinum, methanol, ethanol, carbon monoxide, fuel cell, operando spectroscopy, density functional theory, infrared spectroscopy*

INTRODUCTION

Liquid feed direct methanol and ethanol fuel cells are promising candidates for portable power applications. Alcohols are inexpensive, have limited toxicity, and are liquid at operating temperatures. Methanol and ethanol have high energy densities (3780 kcal/L and 5450 kcal/L respectively) compared to hydrogen (947 kcal/L) at 400 atm.[1] Direct oxidation obviates the need for fuel processing, and thus enables compact system design.[2] Unfortunately these advantages are counterbalanced by the sluggish kinetics of direct alcohol electrooxidation.[3−7] The mechanisms of alcohol oxidation on polycrystalline platinum, single-crystal platinum, and platinum alloys continue to be extensively studied.[4−6,8−17] The exposure of Pt to alcohols at adsorption potentials triggers multistep dehydrogenation processes that yield adsorbed carbon monoxide (CO_{ads}), an intermediate known to bind strongly to Pt surfaces.[18] At high coverages CO_{ads} is primarily atop.[18,19] At lower coverages, both linear and bridge bonded CO_{ads} are comparable.[10] Strategies to optimize the bifunctional mechanism include the use of binary and ternary disordered alloys[20,21] and intermetallics.[22−24] Ethanol electrooxidation kinetics is further exacerbated by the demand for C−C bond cleavage.[5,14,15,25]

The first steps of methanol[4,11] and the ethanol[8,13] oxidative adsorption have been reported:

Methanol

$$Pt + CH_3OH \rightarrow Pt—CH_3OH_{ads}$$

$$Pt—CH_3OH_{ads} \rightarrow Pt—CH_3O_{ads} + H^+ + e^-$$

Ethanol

$$Pt + CH_3CH_2OH \rightarrow Pt—CHOHCH_{3\ ads} + H^+ + e^-$$

Oxidative adsorption processes require an ensemble of surface atoms.[12,26−28] Previous studies of polycrystalline, single crystal, and arc melted alloys[12,26,28] suggest that the oxidative adsorption of methanol requires a 3-atom Pt ensemble for the dehydrogenation process. The additional methylene group in ethanol should increase the number of Pt atoms required for oxidative adsorption. The study of oxidative adsorption in operating liquid feed fuel cells captures the effects of low coordinate surface atoms typical of nanocrystallites,[29,30] and the complex environment of a membrane electrode assembly. The polymer electrolyte has no mobile anions and likely enhances electrocatalysis.[29] Ensemble requirements would be expected to preclude full CO_{ads} coverage on Pt surfaces, with the maximum coverage decreasing as the alcohol molecular weight increases.[3]

In this work, the stripping voltammetry of CO_{MeOH} and CO_{EtOH} in an operating direct alcohol fuel cell were compared to that of CO_{CO}. The stripping voltammetry was correlated to

Special Issue: Electrocatalysis

Received: January 21, 2012
Revised: March 14, 2012
Published: March 16, 2012

   dx.doi.org/10.1021/cs3000478 | ACS Catal. 2012, 2, 701−707

potential dependent infrared (IR) spectra of CO_{ads} (Stark tuning curves[31,32]) obtained by operando spectroscopy of a direct oxidation fuel cell. The experimental data is further rationalized by density functional theory (DFT) calculations of adsorbed methanol and ethanol, and simulations of ensemble requirements for oxidative adsorption of alcohols on Pt (100).

EXPERIMENTAL SECTION

Materials and Fuel Cell Apparatus. The delivery of humidified gases, cell temperature, and the reactant transfer line temperatures were controlled by an EZlab fuel cell test station (NuVant Systems Inc., Crown Point, IN). An external pump (P625 Peristaltic Pump, Instech Laboratories, Inc., Plymouth Meeting, PA) was used for delivery of aqueous methanol, ethanol or Nanopure water.

Membrane electrode assembly (MEA) preparation. MEAs were prepared as previously reported.[33] Briefly, catalyst inks were prepared by dispersing Pt black (Johnson Matthey) in a 5 wt % Nafion ionomer solution (Sigma Aldrich, Milwaukee, WI). The inks were brush painted onto 5 cm^2 areas of Nafion-117 (E.I. DuPont) membranes that were supported on a controlled temperature (70 °C) vacuum table (NuVant Systems Inc.). The anode and cathode Pt loadings were 4 mg/cm^2. Toray carbon paper (Toray Industries, Tokyo, Japan) was used as current collecting gas diffusion layers (GDLs). The 5 cm^2 cell fuel cell (NuVant Systems) was torqued to 25 in. lbs., and then purged with humidified N_2 (Grade 5, Middlesex Gases & Technologies Inc., Everett, MA) while ramping to system temperatures (e.g., cell 30 °C, working electrode (WE) humidifier 35 °C, working electrode transfer line 40 °C, counter/reference electrode (CE/RE) humidifier 25 °C, and counter/reference electrode transfer line 30 °C. The electrode labels in these temperature settings are identical to those of the electrode cleaning process and stripping voltammetry temperature settings. The electrode connections are switched to opposite sides of the fuel cell after fuel cell conditioning.). The use of the CE as a hydrogen reference electrode (CE/RE) has been described.[34,35] After attainment of steady state conditions, the cell bolts were torqued to 35 in. lbs.

Fuel Cell Conditioning. The MEA working electrodes were subjected to stripping voltammetry of CO derived from humidified CO (balanced Nitrogen) and 0.5 M methanol and ethanol. Prior to the stripping voltammetry, each MEA was conditioned with 50 sccm of humidified H_2 (UHP, Middlesex Gases & Technologies Inc., Everett, MA) at the CE/RE and 100 sccm of humidified air at the WE (cell at 50 °C), WE humidifier at 45 °C, WE humidifier transfer line 50 °C, CE/RE humidifier 55 °C, and CE/RE humidifier transfer line 60 °C. The potential was scanned between 800 mV and 600 mV until steady state was attained.

Electrode Cleaning Process. The anode and cathode were purged with humidified N_2. The temperatures were set to: cell 30 °C, WE humidifier 35 °C, WE transfer line 40 °C, CE/RE humidifier 25 °C, and CE/RE transfer line 30 °C. The CE/RE flow was set to 50 sccm humidified H_2 for 50 cycles at 100 mV/s and then 20 scans at 20 mV/s from 0 to 1.0 V.

CO Stripping Voltammetry. The WEs were dosed (60 sccm, 15 min) at 200 mV with humidified 5% CO balanced N_2 (Grade 5, The American Gas Group, Toledo, OH) while humidified H_2 (50 sccm) was delivered to the CE/RE. The WE stream was switched to humidified N_2 at 200 mV for 30 min. The potential was ramped to 0 V vs reference hydrogen electrode (RHE). Stripping voltammetry background waves were obtained by cycling from 0 to 1.0 V (10 mV/s) for three cycles. After background or stripping waves were obtained, the MEAs were electrochemically cleaned. The dose-purge-clean procedures were repeated at 300 mV and 400 mV. The experiments were repeated at 300 mV at cell 50 °C, WE humidifier 55 °C, WE transfer line 60 °C, CE/RE humidifier 45 °C, and CE/RE transfer line 50 °C. The cell shut-down process initiated with reduction of the cell temperature to room temperature while purging with humidified N_2 overnight.

Methanol and Ethanol Stripping Voltammetry. After purging both electrodes with humidified N_2, the WE was switched to 2.5 mL/min of Nanopure H_2O (Milli-Q, Billerica, MA) and the CE/RE was switched to dry N_2 for at least 20 min. The WE transfer line and cell were set to 30 °C while the CE/RE transfer line was set to 25 °C. Dry H_2 (50 sccm) at the CE/RE and 2.5 mL/min nanopure H_2O at the WE were delivered during electrochemical cleaning.

Dosing was carried out with 0.50 mL/min of 0.5 M methanol or 0.5 M ethanol (99.8% Methanol, ≥ 99.5% Ethanol, Sigma-Aldrich) at the WE with dry H_2 (50 sccm) at the CE/RE. After 20 min the WE was switched to 2.5 mL/min nanopure H_2O and purged for 30 min. The cell was held during the full dose/purge procedure at 200 mV and then scanned back to 0 mV (20 mV/s). The CO_{ads} stripping was carried out from 0 to 1.0 V for 7 cycles followed by electrode electrochemical cleaning. Dose-purge-clean procedures were repeated twice for MeOH and EtOH with the cell at 300 mV and 400 mV. The dose-purge-cleaning process was repeated at 300 mV with the cell, WE and CE/RE transfer lines set to 50 °C.

Operando Reflectance IR Spectroscopy of Membrane Electrode Assemblies. Operando spectroscopy was carried out as previously reported[33,36] with an upgraded spectroscopy cell (Figure 1).

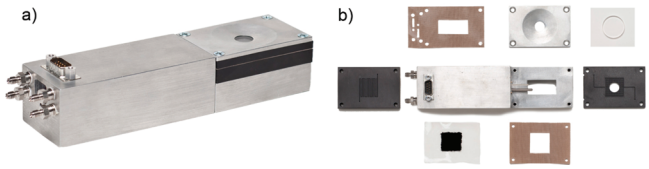

Figure 1. IR-XAS operando fuel cell: (a) fully assembled IR-XAS cell. (b) Center; slider assembly with exposed thermistor and fuel cell support platform. Clockwise (in order of assembly from top center): top plate, CaF_2 disk, WE flow field, WE MEA gasket, MEA, CE/RE flow field, slider housing gasket, slider housing (center).

The slider assembly (Figure 1b, center) interfaces to a diffuse reflectance accessory (Pike Technologies, Madison, WI). The rectangular cut-out in the slider accommodates transmission X-ray absorption spectroscopy (the beam path includes only graphite components and the MEA). The slider housing gasket folds at 90 degrees to accommodate electronic components and flow paths originating from the 9-pin connector and Swagelok fittings respectively. A Vertex 70 (Bruker, Billerica, MA) equipped nitrogen cooled MCT detector accommodates the loaded diffuse reflectance accessory.

Hydrogen (50 sccm) was delivered to the CE flow field. Methanol or ethanol vapor was supplied to the WE flow field via syringe pump injection of 3.33 μL/min of 10 M alcohol into a gas chromatograph (no column) flash evaporator using 60 sccm N_2 as a carrier gas. The cell (50 °C) was equilibrated under these conditions for 1−2 h. FTIR spectra were obtained by averaging 100 scans at 4 cm^{-1} resolution. A reference

dx.doi.org/10.1021/cs3000478 | ACS Catal. 2012, 2, 701−707

spectrum was obtained at 0 V before potential dependent spectra were acquired at 100 mV increments from 0 to 1.0 V. Additional details concerning the operando spectroscopy setup have been reported.[33,36,37]

Data Analysis. Data was processed using Origin 8.1 (OriginLab, Northampton, MA). The CO_{ads} stripping wave integrals for the CO_{CO} and CO_{MeOH} were determined by calculating the integral of the CO_{ads} peak in the first 0−1.0 V scan using clean-electrode data as the baseline. The potential range for integration was determined by locating the potentials where the CO_{ads} peak intersects the clean electrode scan. The hydrogen desorption integrals (for the gaseous CO adsorption measurements) were obtained similarly using the first scan (where H is suppressed by CO_{ads}) as the baseline, and calculating the integral between the intersection of the two scans. Hydrogen desorption integrals for MeOH and EtOH were calculated using a straight baseline at a current that matched the double layer current value of each respective experiment, then integrating between the potentials where the hydrogen wave intersected with the straight-line baseline. The CO_{ads} (from EtOH) integral was determined using a straight-line baseline between the potential values around the peak where the derivative was zero. The clean electrode scan could not be used as the baseline for CO_{ads} from EtOH because the currents in the Pt−O regime of the scan slowly declined following each full potential scan: The upper potential limit of the CO_{ads} peak did not intersect with the clean electrode scan. To ensure that the difference in CO_{ads} peak integration methods for MeOH and EtOH were not substantive, the MeOH CO_{ads} peaks were also integrated using the baseline method as used for EtOH. The results (Figure 1, Supporting Information) confirm this. The electrochemically active surface areas (EASAs) were determined using the literature values of 420 $\mu C/cm^2$ for CO_{ads} and 210 $\mu C/cm^2$ for H.[19]

Density Functional Theory Calculations. Pt (100) was modeled as a three-layer (13)(12)(1) Pt_{26} cluster with a lattice parameter of 3.924 Å. A three-layer model was used in our previous calculations of CO stretching frequencies on spin optimized Pt and PtRu alloy model surfaces,[38] and also compared to slab models.[39] Plans to extend this work to the vibrational spectroscopy of adsorbed molecular fragments of methanol and ethanol motivated use of the same three-layer clusters for consistency with the previous CO/Pt and Co/PtRu studies. Deprotonated methanol, ethanol, and CO were adsorbed on the Pt cluster. Jaguar 7.5 (Schrödinger Inc., Portland, OR) was used for DFT calculations. Unrestricted DFT[40−42] under the hybrid X3LYP[43,44] functional was used to optimize methanol and ethanol fragment adsorption geometries. For each cluster, the ground state multiplicity is iteratively determined by calculating the SCF energy for various spin multiplicity values.[45] The selected spin-optimized cluster is then geometrically optimized by letting the carbon, oxygen, and hydrogen atoms relax, while the Pt atoms remain locked.

RESULTS AND DISCUSSION

Figure 2 shows how the hydrogen adsorption−desorption waves obtained with a flooded MEA differ from those obtained in a humidified gas environment. Hydrogen evolution does not occur until 0 V vs the CE/RE at a flooded electrode, and at more positive potentials (e.g., 0.09 V vs RHE) in the humidified environment. Thus, electrochemically active areas determined by integrating the underpotentially adsorbed hydrogen on MEAs exposed to humidified gases are underestimated because the truncated limits of integration (Figure 3).[46] Truncation of the integration limits (i.e., not extending to 0 V) is common.[3,47] Carter et al.[46] and Edmundson et al.[48] also showed that at a flooded MEA, hydrogen evolution occurs very near to 0 V, while at electrodes exposed to humidified gases, hydrogen evolution occurs at more positive potentials. The use of fully flooded electrodes for more accurate and consistent EASA determination obviates the need for the elaborate corrections required when using data from humidified gas environments. In this study, the stripping voltammetry of CO_{MeOH} and CO_{EtOH} was conducted in a liquid feed fuel cell flooded environment.

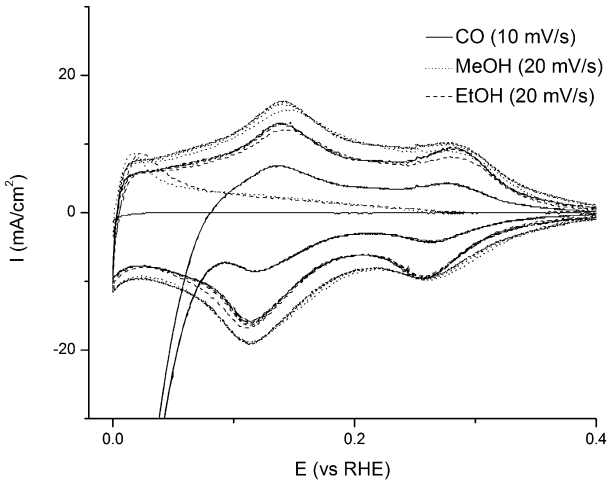

Figure 2. Hydrogen UPD region on Pt for CO_g (3 scans), 0.5 M MeOH (7 scans), and 0.5 M EtOH (7 scans) at 300 mV adsorption potential at 30 °C cell temperature. The scans start immediately after dosing and continue until electrode is clean. The CO scan (solid line) shows hydrogen evolution at more positive potentials in the humidified environment.

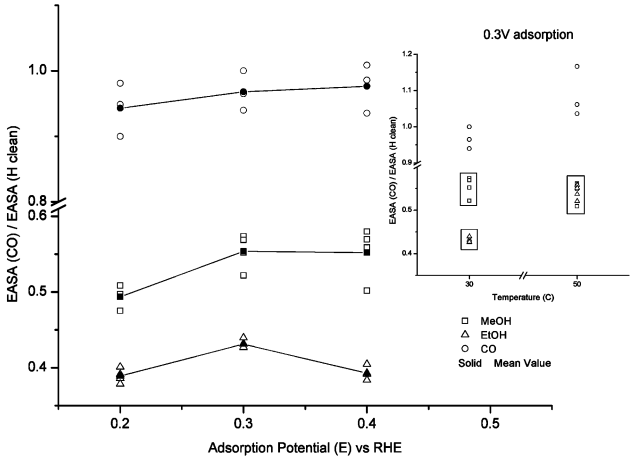

Figure 3. Fractional coverage of CO on Pt (100) from directly dosed CO, 0.5 M MeOH, and 0.5 M EtOH at 200, 300, and 400 mV adsorption potentials at 30 °C fuel cell operation. Inset graph shows the three adsorbates at 300 mV adsorption potential at 30 and 50 °C cell temperature.

The oxidative adsorption and the stripping voltammetry were done at 30 and 50 °C operating temperatures. Figure 3 shows that the fractional coverages (black lines averaged over the 4 MEAs) for CO_{CO}, CO_{MeOH}, and CO_{EtOH} are 0.94, 0.49, and

dx.doi.org/10.1021/cs3000478 | ACS Catal. 2012, 2, 701−707

0.39, respectively, at 0.2 V. The coexistence of bridge-bound CO_{ads} reduces the fractional coverage CO_{CO} to below 1, as is observed. Jusys et al. reported that the CO_{MeOH} on carbon supported Pt surfaces was about half of full coverage at 300 mV,[3] consistent with our value of 0.55 at 30 °C. The ratio of CO_{EtOH}/CO_{MeOH} at 0.2 V and 30 °C is 0.79 ± 4%. At 50 °C the CO_{EtOH} and CO_{MeOH}, within the spread of the data, are identical: The ethanol ensemble requirements may be relaxed because of more facile rotation along the ethanol C−C bond. The effect of increased CO coverage (due to the relaxation of site requirements) on the overall kinetics of ethanol oxidation is not addressed in this work. An excellent review of methanol and ethanol electrooxidation kinetics provides guidance toward addressing this in future studies.[16] The dependence of the breakpoint features at 0.3 V (30 °C data), on the adsorbate size will be discussed later.

Figure 4 shows the stripping voltammetry dependence on fuel cell operating temperature. At higher temperature the oxidation potential shifts negatively, consistent with Arrhenius kinetics and in agreement with previous studies.[5−7,27,49−54]

Alcohol adsorption on the Pt surfaces has been modeled using DFT.[9,15] Our calculations, visualized using Maestro 9.2 (Schrödinger, Portland, OR), show the unrestricted DFT geometry optimization for the first step of methanol and ethanol adsorption on a Pt (100) surface (Figure 5). Pt (100) has been shown to be the most active surface for MeOH oxidation.[15,55]

The Pt (100) model shows methanol fully blocking two Pt atoms. Ethanol fully blocks two atoms and sterically hinders two other Pt atoms as well. The Pt (100) face is the most open structure. Thus the ensemble requirements may be higher on other crystallite facets. CO coverage was simulated using a 61 atom Pt (100) layer and ensemble requirements of 2 and 3 (non-linear, Figure 5 right) atoms. This simple model emphasizes effects due solely to ensemble requirements. The Pt atoms were numbered and selected by a random number generator. If the selected atom was included in a required ensemble, a CO_{ads} was placed on the selected atom. This process is continued until no ensembles remain. An animated PowerPoint file demonstrating the simulation process is in the Supporting Information. Table 1 in the Supporting Information provides simulation results. An average CO_{EtOH}/CO_{MeOH} was calculated to be 0.78 ± 4% in comparison to the experimentally determined value of 0.79 ± 4% (Figure 3, 200 mV at 30 °C). Clearly Johnson Matthey catalyst surfaces are not entirely Pt (100) but this simple method of approximation suggests that the measured values and conclusions are within reason.

Potential dependent IR spectra, with steady state vapor phase aqueous methanol or ethanol flash evaporated to the anode, are shown in Figure 6. The peak heights for CO_{MeOH} are larger than for CO_{EtOH} at all adsorption potentials, and both systematically increase with potential. The CO stretching frequencies for CO_{MeOH} occur at higher wavenumbers because of the higher coverage (relative to CO_{EtOH}) on the Pt. An important distinction between the stripping voltammetry and the Stark tuning experiments is that the Stark tuning experiments are done with steady state delivery of gaseous fuel.

Figure 7 shows the Stark tuning curves for CO_{MeOH} and CO_{EtOH}. The CO_{MeOH} Stark tuning curve is shifted about 12 wavenumbers up relative to that of ethanol because of the higher dipole−dipole coupling associated with higher CO_{ads} coverage. The Stark tuning rates are 1.9 cm^{-1} V^{-1} and 6.5 cm^{-1} V^{-1} between 600 mV and 1 V for C_{MeOH} and CO_{EtOH},

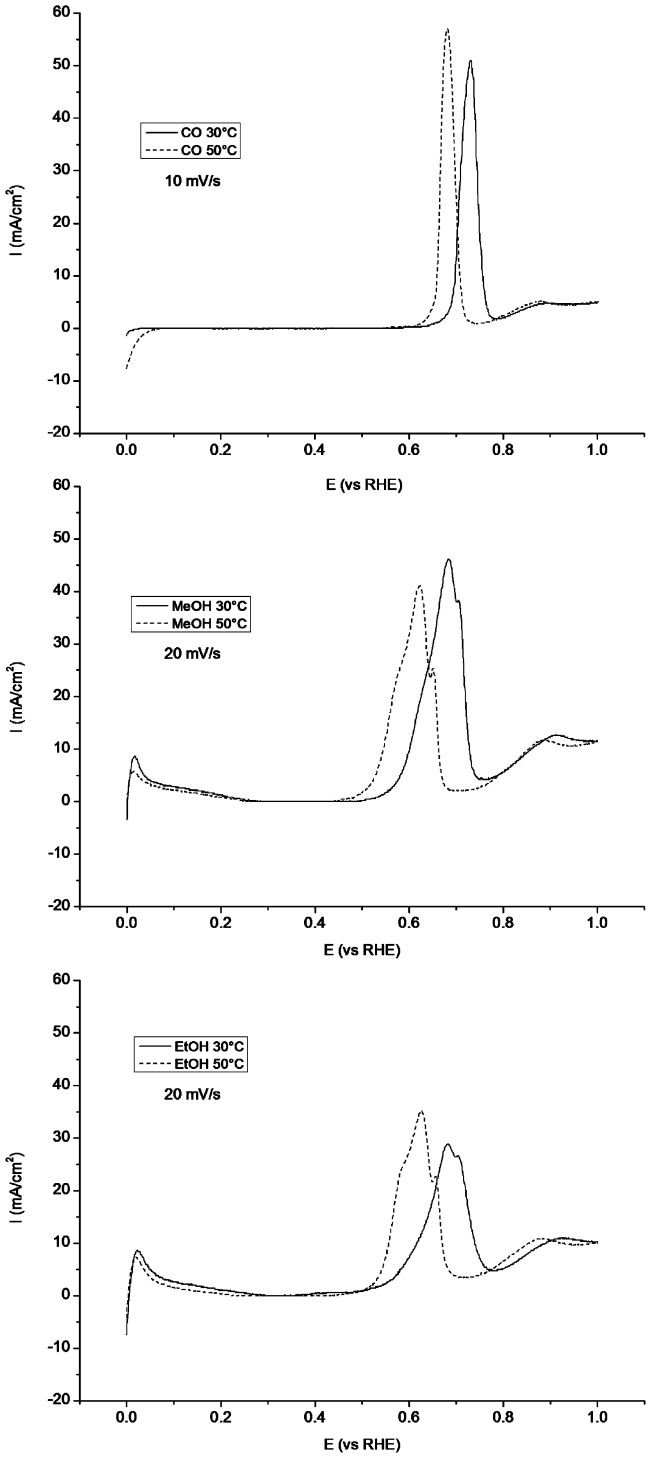

Figure 4. Temperature of stripping voltammetry for CO_{ads} obtained from CO_g, 0.5 M MeOH, and 0.5 M EtOH at 300 mV adsorption potential at 30 and 50 °C cell temperature.

respectively. The substantially lower Stark tuning rates in comparison to single crystalline and polished polycrystalline Pt is consistent with our previous studies of CO_{ads} Stark tuning on membrane electrode assembly Pt[56] and on arc-melted alloys.[57] The Stark tuning rates are sensitive to surface conditions and potential, and not simply a bulk material property. The Nafion overlayer provides a unique environment for MEA incorporated catalysts[29,33] and may play a role in the lowering of Stark tuning rates of CO on fuel cell electrodes.[58]

dx.doi.org/10.1021/cs3000478 | ACS Catal. 2012, 2, 701−707

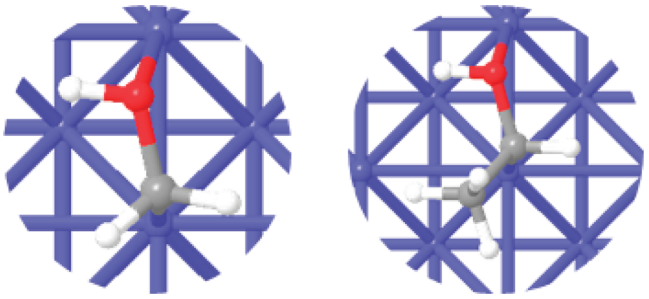

Figure 5. Adsorption of MeOH (left) and EtOH (right) on Pt (100). Red atom is oxygen, gray carbon, and white hydrogen.

The CO_{MeOH} Stark tuning curve of Figure 7 (with steady state flow) correlates perfectly to our previously reported CO_{CO} Stark tuning curve from a CO dosed and purged MEA. Both curves initiated at 2082 cm^{-1}. In the previous work there was a drop of 10 cm^{-1} in the stretching frequency at 350 mV corresponding to the onset of CO oxidation (Figure 2 of reference 31). In this work that precipitous drop is absent because the steady state flash evaporation of methanol/water replenishes the CO_{MeOH}. In the case of CO_{EtOH} the drop

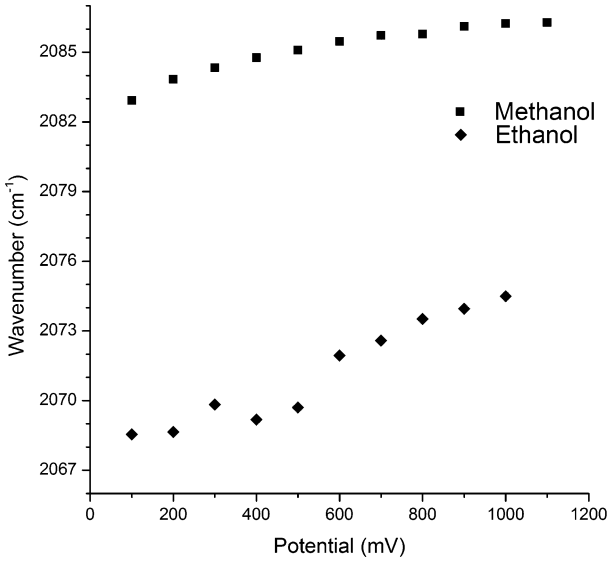

Figure 7. Stark tuning curve of CO_{MeOH} and CO_{EtOH} in a gas fed fuel cell at 50 °C.

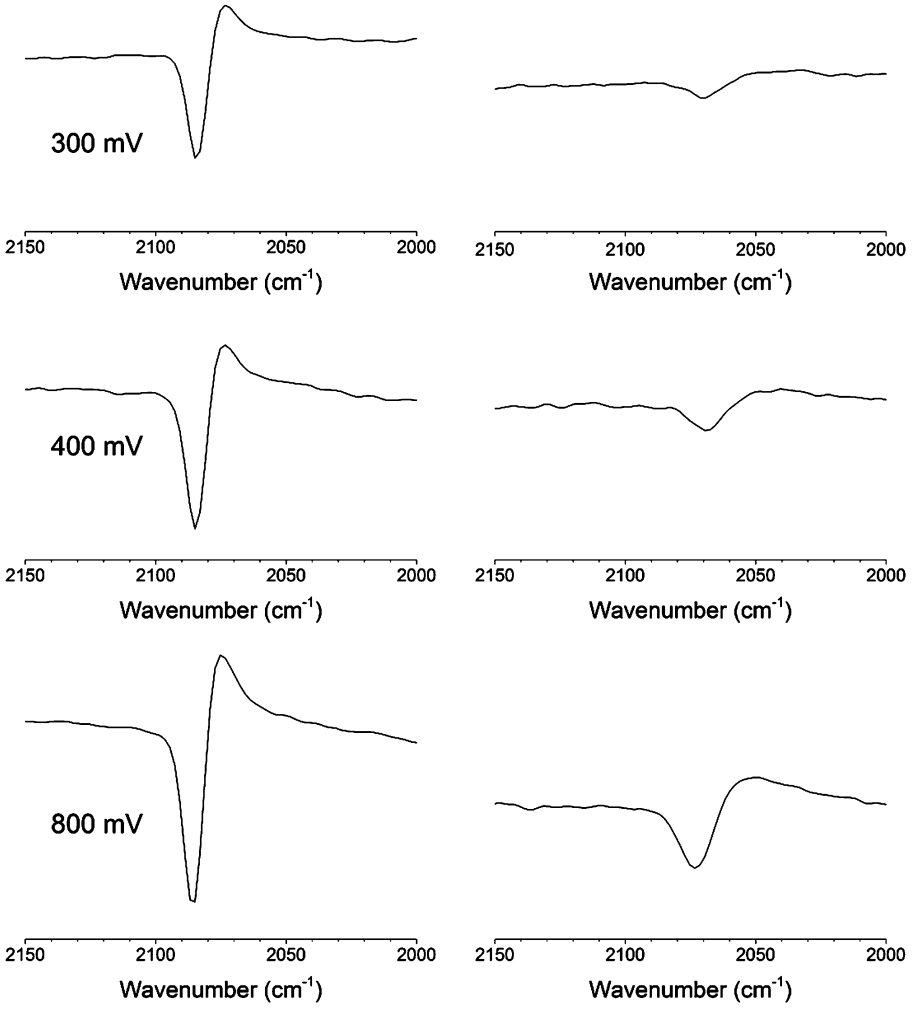

Figure 6. Operando IR spectra of CO at selected potentials from oxidized methanol (left) and ethanol (right).

dx.doi.org/10.1021/cs3000478 | ACS Catal. 2012, 2, 701−707

appears (Figure 7 lower curve) in spite of the steady state delivery of ethanol/water and is attenuated (3−4 cm^{-1}). This may be related to the lower CO_{EtOH} coverage. Complex Stark tuning of CO on Pt has been thoroughly discussed.[33,59] More work is needed to fully understand the correlation between gas fed and liquid feed fuel cells.

CONCLUSIONS

The stripping voltammetry of CO oxidatively adsorbed from methanol and ethanol on Pt catalysts in an operating liquid feed direct oxidation fuel cell were obtained at 30 and 50 °C. A ratio of CO_{EtOH}/CO_{MeOH} of 0.79 was obtained at 30 °C. The simulation of oxidative adsorption of methanol and ethanol on defect free Pt (100), assuming ensemble site requirements of 2 and 3 surface atoms, respectively, yields a ratio of CO_{EtOH}/CO_{MeOH} of 0.78. The fortuitous similarity of the simulation and experimental results suggests that the use of the very open structure of Pt (100) for the simulations has overall adsorption properties similar to the low coordinate atoms of nanocrystalline catalysts. The experimental and simulation results suggests that a reasonable estimate for the ensemble site requirements for oxidative adsorption of ethanol is 50% higher than for methanol in an operating liquid feed fuel cell at 30 °C. At 50 °C the CO_{EtOH}/CO_{MeOH} ratio approaches unity, suggesting a relaxation of site requirements for ethanol at higher temperature. The cooperative effects of site-requirement relaxation on overall ethanol electrooxidation kinetics are under study.

ASSOCIATED CONTENT

Supporting Information

Figure 1: Graph of fractional coverages of CO_{CO}, CO_{MeOH}, CO_{EtOH} alternative calculations; Table 1: Random number ensemble simulation results with mean and standard deviations. This material is available free of charge via the Internet at http://pubs.acs.org.

AUTHOR INFORMATION

Corresponding Author

*Phone: 1-617-373-7526. Fax: 1-617-373-8795. E-mail: e.smotkin@neu.edu.

Funding

Funding for this project was provided by NuVant Systems Inc.

Notes

The authors declare no competing financial interest.

REFERENCES

(1) Engel, T.; Reid, P. *Physical Chemistry*, 2nd ed.; Pearson Prentice Hall: Upper Saddle River, NJ, 2010; pp 1001−1016.
(2) Ueda, H.; Fukuda, S. Direct Methanol Fuel Cell. U.S. Patent 7,803,490, Sep 28, 2010.
(3) Jusys, Z.; Behm, R. J. *J. Phys. Chem. B* **2001**, *105*, 10874−10883.
(4) Lei, H. W.; Suh, S.; Gurau, B.; Workie, B.; Liu, R. X.; Smotkin, E. S. *Electrochim. Acta* **2002**, *47*, 2913−2919.
(5) Sen Gupta, S.; Singh, S.; Datta, J. *Mater. Chem. Phys.* **2010**, *120*, 682−690.
(6) Otomo, J.; Nishida, S.; Takahashi, H.; Nagamoto, H. *J. Electroanal. Chem.* **2008**, *615*, 84−90.
(7) Sun, S.; Halseid, M. C.; Heinen, M.; Jusys, Z.; Behm, R. J. *J. Power Sources* **2009**, *190*, 2−13 , and references therein.
(8) Vigier, F.; Rousseau, S.; Coutanceau, C.; Leger, J.-M.; Lamy, C. *Top. Catal.* **2006**, *40*, 111−121.
(9) Neurock, M.; Janik, M.; Wieckowski, A. *Faraday Discuss.* **2008**, *140*, 363−378.
(10) Fan, Q. B.; Pu, C.; Ley, K. L.; Smotkin, E. S. *J. Electrochem. Soc.* **1996**, *143*, L21−L23.
(11) Frelink, T.; Visscher, W.; Vanveen, J. A. R. *Surf. Sci.* **1995**, *335*, 353−360.
(12) Gasteiger, H. A.; Markovic, N.; Ross, P. N.; Cairns, E. J. *J. Phys. Chem.* **1993**, *97*, 12020−12029.
(13) Iwasita, T.; Pastor, E. *Electrochim. Acta* **1994**, *39*, 531−537.
(14) Colmati, F.; Tremiliosi-Filho, G.; Gonzalez, E. R.; Berna, A.; Herrero, E.; Feliu, J. M. *Phys. Chem. Chem. Phys.* **2009**, *11*, 9114−9123.
(15) Wang, H.-F.; Liu, Z.-P. *J. Am. Chem. Soc.* **2008**, *130*, 10996−11004.
(16) Koper, M. T. M.; Lai, S. C. S.; Herrero, E. In *Fuel Cell Catalysis: A Surface Science Approach*; Koper, M. T. M., Ed.; Wiley: Hoboken, NJ, 2009; pp 159−207.
(17) Herrero, E.; Franaszczuk, K.; Wieckowski, A. *J. Phys. Chem.* **1994**, *98*, 5074−5083.
(18) Gasteiger, H. A.; Markovic, N.; Ross, P. N.; Cairns, E. J. *J. Phys. Chem.* **1994**, *98*, 617−625.
(19) Brett, D. J. L.; Atkins, S.; Brandon, N. P.; Vesovic, V.; Vasileiadis, N.; Kucernak, A. R. *J. Power Sources* **2004**, *133*, 205−213 , and references therein.
(20) Ley, K. L.; Liu, R.; Pu, C.; Fan, Q.; Leyarovska, N.; Segre, C.; Smotkin, E. S. *J. Electrochem. Soc.* **1997**, *144*, 1543−1548.
(21) Gurau, B.; Viswanathan, R.; Liu, R. X.; Lafrenz, T. J.; Ley, K. L.; Smotkin, E. S.; Reddington, E.; Sapienza, A.; Chan, B. C.; Mallouk, T. E.; Sarangapani, S. *J. Phys. Chem. B* **1998**, *102*, 9997−10003.
(22) Blasini, D. R.; Rochefort, D.; Fachini, E.; Alden, L. R.; DiSalvo, F. J.; Cabrera, C. R.; Abruna, H. D. *Surf. Sci.* **2006**, *600*, 2670−2680.
(23) Oana, M.; Hoffmann, R.; Abruña, H. D.; DiSalvo, F. J. *Surf. Sci.* **2005**, *574*, 1−16.
(24) Casado-Rivera, E.; Volpe, D. J.; Alden, L.; Lind, C.; Downie, C.; Vázquez-Alvarez, T.; Angelo, A. C. D.; DiSalvo, F. J.; Abruña, H. D. *J. Am. Chem. Soc.* **2004**, *126*, 4043−4049.
(25) Kowal, A.; Li, M.; Shao, M.; Sasaki, K.; Vukmirovic, M. B.; Zhang, J.; Marinkovic, N. S.; Liu, P.; Frenkel, A. I.; Adzic, R. R. *Nat. Mater.* **2009**, *8*, 325−330.
(26) Cuesta, A. *J. Am. Chem. Soc.* **2006**, *128*, 13332−13333.
(27) Gasteiger, H. A.; Markovic, N.; Ross, P. N.; Cairns, E. J. *J. Electrochem. Soc.* **1994**, *141*, 1795−1803.
(28) Gasteiger, H. A.; Markovic, N.; Ross, P. N. Jr.; Cairns, E. J. *Electrochim. Acta* **1994**, *39*, 1825−1832.
(29) Liu, L.; Viswanathan, R.; Liu, R.; Smotkin, E. S. *Electrochem. Solid-State Lett.* **1998**, *1*, 123−125.
(30) Stoupin, S.; Chung, E.-H.; Chattopadhyay, S.; Segre, C. U.; Smotkin, E. S. *J. Phys. Chem. B* **2006**, *110*, 9932−9938.
(31) Zou, S.; Weaver, M. J. *J. Phys. Chem.* **1996**, *100*, 4237−4242.
(32) Inkaew, P.; Zhou, W.; Korzeniewski, C. *J. Electroanal. Chem.* **2008**, *614*, 93−100.
(33) Kendrick, I.; Kumari, D.; Yakaboski, A.; Dimakis, N.; Smotkin, E. S. *J. Am. Chem. Soc.* **2010**, *132*, 17611−17616.
(34) Gurau, B.; Smotkin, E. S. *J. Power Sources* **2002**, *112*, 339−352.
(35) Rivera, H.; Lawton, J. S.; Budil, D. E.; Smotkin, E. S. *J. Phys. Chem. B* **2008**, *112*, 8542−8548.
(36) Lewis, E. A.; Kendrick, I.; Jia, Q. Y.; Grice, C.; Segre, C. U.; Smotkin, E. S. *Electrochim. Acta* **2011**, *56*, 8827−8832.
(37) Lewis, E. A.; Segre, C. U.; Smotkin, E. S. *Electrochim. Acta* **2009**, *54*, 7181−7185.
(38) Dimakis, N.; Iddir, H.; Díaz-Morales, R. R.; Liu, R.; Bunker, G.; Chung, E.-H.; Smotkin, E. S. *J. Phys. Chem. B* **2005**, *109*, 1839−1848.
(39) Dimakis, N.; Cowan, M.; Hanson, G.; Smotkin, E. S. *J. Phys. Chem. C* **2009**, *113*, 18730−18739.
(40) Hohenberg, P.; Kohn, W. *Phys. Rev.* **1964**, *136*, B864−B871.
(41) Kohn, W.; Sham, L. J. *Phys. Rev.* **1965**, *140*, A1133−A1138.
(42) Parr, R. G.; Yang, W. *Density Functional Theory of Atoms and Molecules*; Oxford University Press: New York, 1989.
(43) Xu, X. *J. Chem. Phys.* **2005**, *122*, 014105.
(44) Xu, X.; Goddard, W. A. *Proc. Natl. Acad. Sci. U.S.A.* **2004**, *101*, 2673−2677.

(45) Kua, J.; Goddard, W. A. *J. Am. Chem. Soc.* **1999**, *121*, 10928−10941.
(46) Carter, R. N.; Kocha, S. S.; Wagner, F.; Fay, M.; Gasteiger, H. A. *ECS Trans.* **2007**, *11*, 403−410.
(47) McGrath, P.; Fojas, A. M.; Reimer, J. A.; Cairns, E. J. *Chem. Eng. Sci.* **2009**, *64*, 4765−4771.
(48) Edmundson, M.; Busby, F. C. *ECS Trans.* **2011**, *41*, 661−671.
(49) Seiler, T.; Savinova, E. R.; Friedrich, K. A.; Stimming, U. *Electrochim. Acta* **2004**, *49*, 3927−3936.
(50) Behm, R. J.; Jusys, Z. *J. Power Sources* **2006**, *154*, 327−342.
(51) Aricò, A. S.; Baglio, V.; Di Blasi, A.; Modica, E.; Antonucci, P. L.; Antonucci, V. *J. Electroanal. Chem.* **2003**, *557*, 167−176.
(52) Camargo, A. P. M; Previdello, B. A. F.; Varela, H.; Gonzalez, E. R. *Quim. Nova* **2010**, *33*, 2143−2147.
(53) Herrero, E.; Álvarez, B.; Feliu, J. M.; Blais, S.; Radovic-Hrapovic, Z.; Jerkiewicz, G. *J. Electroanal. Chem.* **2004**, *567*, 139−149.
(54) Kardash, D.; Huang, J.; Korzeniewski, C. *Langmuir* **1999**, *16*, 2019−2023.
(55) Xia, X. H.; Iwasita, T.; Ge, F.; Vielstich, W. *Electrochim. Acta* **1996**, *41*, 711−718.
(56) Liu, R.; Iddir, H.; Fan, Q.; Hou, G.; Bo, A.; Ley, K. L.; Smotkin, E. S.; Sung, Y. E.; Kim, H.; Thomas, S.; Wieckowski, A. *J. Phys. Chem. B* **2000**, *104*, 3518−3531.
(57) Bo, A.; Sanicharane, S.; Sompalli, B.; Fan, Q.; Gurau, B.; Liu, R.; Smotkin, E. S. *J. Phys. Chem. B* **2000**, *104*, 7377−7381.
(58) Smotkin, E. S. In *In-situ Spectroscopic Studies of Adsorption at the Electrode and Electrocatalysis*; Sun, S. G., Christensen, P. A., Wieckowski, A., Eds.; Elsevier Science B.V.: Amsterdam, The Netherlands, 2007; pp 247−272.
(59) Stamenkovic, V.; Chou, K. C.; Somorjai, G. A.; Ross, P. N.; Markovic, N. M. *J. Phys. Chem. B* **2004**, *109*, 678−680.

NOTE ADDED AFTER ASAP PUBLICATION

After this paper was published online March 29, 2012, a correction was made to the Supporting Information PowerPoint file. The corrected version was reposted March 30, 2012.